

Cs-Promoted Ag(111): Model Studies of Selective Ethylene Oxidation Catalysts

Charles T. Campbell

Chemistry Division, Los Alamos National Laboratory, Los Alamos, New Mexico 87545
(Received: June 28, 1985; In Final Form: August 30, 1985)

The role of cesium promoters in silver catalysts for the selective epoxidation of ethylene ($C_2H_4 + \frac{1}{2}O_2 \rightarrow C_2H_4O$) has been studied by using adsorbed cesium on the surface of clean Ag(111) as a model catalyst. The experiments are performed in an apparatus that allows rapid transfer of the catalyst between an ultrahigh vacuum chamber for surface analysis (XPS, AES, LEED, TDS) and a high-pressure microreactor for kinetic measurements. At 300 K, Cs adsorbs on Ag(111) with strong lateral Cs-Cs repulsions, giving rise to a series of LEED patterns and a very broad (300-800 K) thermal desorption spectrum. The surface saturates in a $p(2 \times 2)$ structure, interpreted as a close-packed Cs layer with $\theta_{Cs} = 0.25$. Multilayers of Cs desorb at ~ 325 K. Dosing with Cs makes a Ag(111) catalyst that is less active but more selective for epoxidation at low conversion than clean Ag(111). Under reaction conditions, the Cs is converted to a surface cesium "oxide" ($\sim CsO_3$), which exists in islands of LEED structure $(2\sqrt{3} \times 2\sqrt{3})R30^\circ$. This structure decomposes at ~ 610 K in thermal desorption, yielding gaseous Cs and O_2 . Some Cs moves into the bulk during the reaction, desorbing as Cs above 700 K.

I. Introduction

The selective oxidation of ethylene to ethylene epoxide (also known as ethylene oxide) is of an important industrial catalytic reaction. It is a prototype for fundamental study of kinetically controlled selectivity in catalysis. The reaction is performed on a Ag catalyst, typically supported on $\alpha-Al_2O_3$. Cesium is a common additive in catalyst preparation. Very good reviews of the use of alkali promoters in these catalysts appear in recent patents^{1a,b} and a review paper.^{1c} From that work, it appears that proper Cs addition leads to higher selectivity but not necessarily higher activity. This is to be contrasted with earlier work²⁻⁴ that suggested that electropositive additives generally decrease the selectivity and increase the activity for CO_2 formation. The use of Cs to enhance selectivity has a number of possible explanations. The further oxidation of the ethylene oxide (EtO) product to CO_2 occurs at high conversions, and it is thought to be initiated by the isomerization of EtO to acetaldehyde.^{5,6} Since the support material (e.g., Al_2O_3) is very active in this isomerization,^{7,8} practitioners have sometimes argued that Cs acts to block acidic sites on the surface of the support, thereby inhibiting isomerization and further oxidation of the product EtO. Recently, Grant and Lambert have shown that this isomerization also occurs on pure Ag, and that Cs addition inhibits this reaction on the Ag surface as well.⁹ They suggest that isomerization on supported catalysts is metal-dominated.

In our continuing program to understand fundamental details of the ethylene epoxidation reaction over Ag, we have shown that Ag(111) and Ag(110) are excellent kinetic models of real-world Ag catalysts in terms of the effects of temperature, reaction pressures, and chlorine additives upon the rates and selectivity.¹⁰⁻¹⁵

In the present work, we investigate the effect of added Cs upon the rate and selectivity for ethylene epoxidation at low conversions over a Ag(111) surface. We find that Cs decreases the activity but can increase the selectivity. This compares with a recent study by Grant and Lambert,¹⁶ where they found under lower pressures that both the selectivity and activity could be increased with Cs addition to Ag(111). It is clear, therefore, that Cs additives have a positive influence on the Ag surface itself, increasing the selectivity in the initial production of EtO and inhibiting its further oxidation to CO_2 . By post-reaction surface analysis, we also elucidate details of the structure and oxidation state of Cs under reaction conditions.

II. Experimental Section

The techniques and equipment have been described in detail previously.^{11,14} In short, the Ag(111) surface was cleaned in ultrahigh vacuum (UHV) and characterized by surface analytical techniques including X-ray photoelectron spectroscopy (XPS), Auger electron spectroscopy (AES), thermal desorption spectroscopy (TDS), and low-energy electron diffraction (LEED). The back and sides of the crystal were passivated to reaction by an inert film.^{11,14} Cesium was then dosed to the front surface by using a vapor deposition source similar to that described previously,¹⁷ where now an SAES Cs getter was resistively heated (~ 900 K) to generate Cs vapor. The Cs adsorption was then characterized by surface techniques as described in section III.1. The Cs/Ag AES ratio was routinely used to calibrate Cs coverages, θ_{Cs} , which are defined relative to the number of Ag(111) surface atoms ($1.38 \times 10^{15} \text{ cm}^{-2}$). The sample was then translated into the evacuated microreactor. The reactor was pressurized with the reaction mixture. The sample was rapidly heated to and maintained at the reaction temperature for 4 min, which is long enough to establish a steady-state reaction rate (limit of low conversion).^{11,14} The sample was rapidly (< 20 s) translated back to UHV at the reaction temperature for post-reaction surface analysis. The gas in the batch microreactor was monitored by gas chromatography to determine the rates of EtO and CO_2 production.

We used a defocused electron beam for AES, as significant beam-damage effects on the Cs overlayers were noticed for a focused electron beam, especially in the presence of oxygen.

III. Results

III.1. Cs Adsorption. Figure 1 shows the variation in Cs-(MNN) and Ag(MNN) AES peak-to-peak intensities and their ratio (I_{Cs}/I_{Ag}) as a function of Cs deposition time at 300 K, for a fixed source temperature of ~ 900 K. The signals vary smoothly with time until about 8 min, after which they remain constant.

(1) (a) Bhasin, M. M.; Elgen, P. C.; Hendrix, C. D. Union Carbide, U.K. Patent Application GB 2 043 481 A. (b) Nielsen, R. P.; LaRoche, J. H. Shell Oil Company, U.S. Patent 3 962 136. (c) Mross, W.-D. *Catal. Rev. Sci. Eng.* **1983**, *25*, 591.

(2) Spath, H. T.; Torkar, K. *J. Catal.* **1972**, *26*, 163.

(3) Margolis, L. Y.; Enikeev, E. K.; Isaev, O. V.; Krylova, A. V.; Kushnerov, M. Y. *Kinet. Katal.* **1962**, *3*, 153.

(4) Verykios, X. E.; Stein, F. P.; Coughlin, R. W. *Catal. Rev. Sci. Eng.* **1980**, *22*, 197.

(5) (a) Ide, Y.; Takagi, T.; Keii, T. *Nippon Kagaku Zasshi* **1965**, *86*, 1249.

(b) Twigg, G. H. *Trans. Faraday Soc.* **1946**, *42*, 284. (c) Twigg, G. H. *Proc. R. Soc. London, Ser. A* **1947**, *188*, 92.

(6) Kenson, R. E.; Lapkin, M. *J. Phys. Chem.* **1970**, *74*, 1493.

(7) Orzechowski, A.; MacCormack, K. E. *Can. J. Chem.* **1954**, *32*, 415 and 432.

(8) Kanoh, H.; Nishimura, T.; Ayame, A. *J. Catal.* **1979**, *57*, 372.

(9) Grant, R. B.; Lambert, R. M. *J. Catal.* **1985**, *93*, 92.

(10) Campbell, C. T. *J. Vac. Sci. Technol.* **1984**, *A2*, 1024.

(11) Campbell, C. T.; Paffett, M. T. *Surf. Sci.* **1984**, *139*, 396.

(12) Campbell, C. T.; Paffett, M. T. *Appl. Surf. Sci.* **1984**, *19*, 28.

(13) Campbell, C. T.; Koel, B. E. *J. Catal.* **1985**, *92*, 272.

(14) Campbell, C. T. *J. Catal.* **1985**, *94*, 436.

(15) Campbell, C. T. "Catalyst Characterization Science", Deviney, M.

L., Gland, J. L., Ed.; American Chemical Society: Washington, DC, 1985; ACS Symp. Series, No. 288, p 210.

(16) Grant, R. B.; Lambert, R. M. *Langmuir* **1985**, *1*, 29.

(17) Paffett, M. T.; Campbell, C. T.; Taylor, T. N.; Srinivasan, S. *Surf. Sci.* **1985**, *154*, 284.

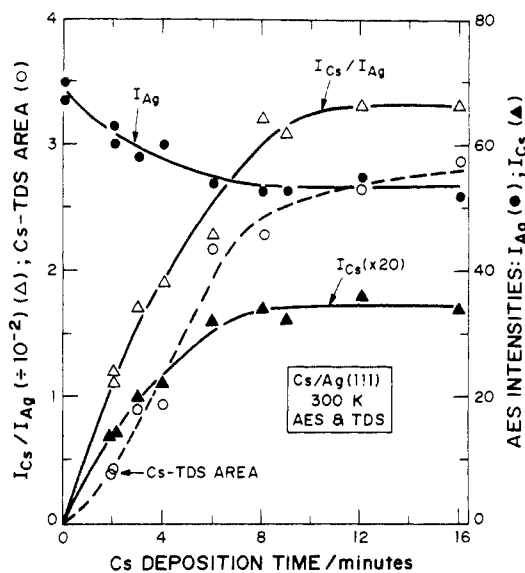


Figure 1. Variation in the Cs (~ 560 eV) and Ag (~ 360 eV) AES signals with Cs deposition time on Ag(111) at 300 K. Also shown is the Cs/Ag AES ratio and the area under Cs TDS spectra such as Figure 2. The signals saturate in a $p(2\times 2)$ LEED pattern which is interpreted as a close-packed monolayer of Cs ($\theta_{Cs} = 0.25$, see below).

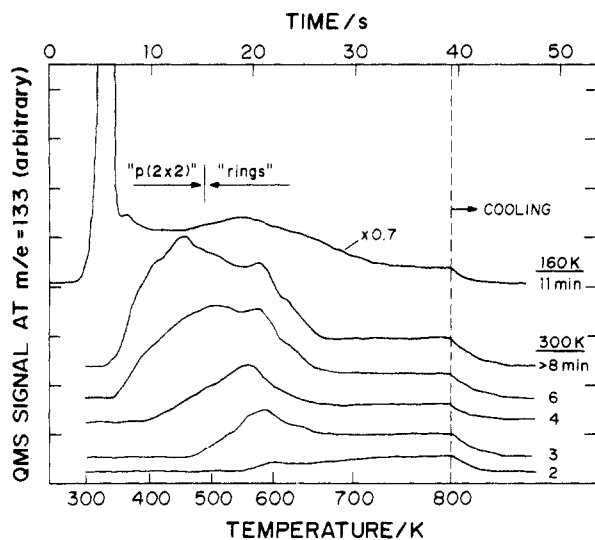


Figure 2. Thermal desorption spectra for various Cs doses at 300 and 160 K. A multilayer is populated at 160 K, desorbing in a sharp peak at ~ 320 K.

This indicates that the surface saturates in Cs, and that multilayers are not stable at 300 K and this dose rate. No distinct breaks are seen in the AES curves to indicate more than one monolayer of Cs.

The Cs TDS of Figure 2 shows that Cs desorbs in a very broad spectrum, beginning at ~ 320 K. The Cs is not completely desorbed by 800 K, the maximum heating temperature, except with extended time. The behavior in Figure 2 is reminiscent of Cs desorption from Ni surfaces,¹⁸ where desorption of the first monolayer extends from 320 to 1100 K in a structured spectrum. The desorption of submonolayer alkali coverages from transition metals is generally very broad, reflecting a strong decrease in the heat of adsorption with coverage.¹⁸⁻²¹ This is due to the strong dipole-dipole repulsion characteristic of these ionic adsorption systems.¹⁸⁻²³ Mutual depolarization accompanies increased

coverage, so that at saturation the monolayer has lost much of its ionic character and is nearly metallic.¹⁸⁻²³

The areas under the TDS curves of Figure 2 are plotted in Figure 1 to show the variation with deposition time. The TDS area grows slowly at first and then accelerates before saturating. This delayed start reflects the fact that $\sim 15\%$ of the saturation coverage is not desorbed by 800 K.

Multilayers of Cs can also be formed on Ag(111) if dosed below 300 K, as shown by the desorption spectrum in Figure 2 after an 11-min dose at 160 K. When several layers are adsorbed, the multilayers desorb in a sharp peak at ~ 320 K. First-order Redhead analysis²⁴ of this peak temperature, assuming a pre-exponential factor for desorption of 10^{13} s⁻¹, yields an activation energy for desorption of 18.6 kcal mol⁻¹. The sublimation energy of bulk Cs is 18.7 kcal mol⁻¹.²⁵

LEED data have helped confirm the structure of Cs overlayers on Ag(111). When the surface is saturated at room temperature or if a higher coverage is adsorbed below 300 K and then partially removed by flashing to 320 K, a $p(2\times 2)$ LEED pattern is observed as shown in Figure 3a. Cooling well below room temperature was necessary to observe the patterns of Figure 2, undoubtedly due to the mobility of Cs. This $p(2\times 2)$ pattern is interpreted as $\theta_{Cs} = 0.25$, i.e., one Cs atom per unit cell, in a hexagonal close-packed monolayer of Cs, rotationally commensurate with the Ag(111) substrate. Note that this structure gives a Cs-Cs interatomic spacing that is 95% of the metallic diameter of Cs.²⁶ Note the extra, faint, half-order spots in Figure 3a that are rotated 30° with respect to the $p(2\times 2)$ pattern. These were observed in some cases. They could be due to domains of a hexagonal overlayer of Cs with about this same lattice spacing, rotated 30° with respect to the substrate. Cesium coverages on clean Ag(111) were taken as proportional to the Cs/Ag AES ratio and calibrated based on this saturation signal for $\theta_{Cs} = 0.25$.

As seen in parts b-d of Figure 3, at lower coverages it is common for the Cs overlayer to lose its rotational registry completely. These patterns were obtained by first saturating the surface at 300 K ($\theta_{Cs} = 0.25$) and then flashing briefly to increasing temperatures to remove some Cs. They show a ring of intensity centered about the (0,0) beam. The radius of the ring decreases with decreasing coverage. As in other work for alkali adsorption,²¹⁻²³ this is interpreted as many domains of hexagonal arrays of Cs, rotationally out of registry with the substrate. The Cs atoms maximize their interatomic spacing. In the figure caption, we list both the Cs coverage obtained by AES (θ_{Cs}) and that obtained from the ring radius (θ_{Cs}^{LEED}) based on this model. The agreement is quite good.

At coverages between about 0.18 and 0.30, other LEED patterns are seen that have a strong $p(2\times 2)$ component or are similar to the $p(2\times 2)$ pattern with split overlayer spots. These patterns will not be discussed due to their complexity. They are referred to as " $p(2\times 2)$ " in Figure 2 for simplicity.

III.2. Reaction Studies for $\theta_{Cs} \leq 0.25$. Steady-state low-conversion ethylene oxidation kinetics were measured on the clean Ag(111) surface containing various predepos of adsorbed Cs. These results are presented as the open symbols in Figures 4 and 5 for 490 and 563 K, respectively. The ethylene (Et) and O₂ pressures were $P_{Et} = 20$ torr and $P_{O_2} = 150$ torr. The rates are expressed as the turnover frequency (TON = molecules produced per site per second), assuming 10^{15} sites on the Ag(111) sample, roughly the number of Ag surface atoms.^{11,14} The selectivity to produce EtO [$S_{EtO} = TON_{EtO} / (TON_{EtO} + \frac{1}{2}TON_{CO_2})$] is not strongly affected but passes through a minimum. A saturation monolayer of Cs ($\theta_{Cs} = 0.25$) is sufficient only to decrease clean surface rates by about 37%.

III.3. Surface Structure after Reaction. After reaction at >490 K, the surface AES showed no adsorbed species except Cs and oxygen. Figure 6 shows the O(KVV) and Cs(MNN) AES spectra

(18) Gerlach, R. L.; Rhodin, T. N. *Surf. Sci.* **1970**, *19*, 403.

(19) Levine, J. D.; Gyftopolous, E. P. *Surf. Sci.* **1964**, *1*, 171.

(20) Lee, S. B.; Weiss, M.; Ertl, G. *Surf. Sci.* **1981**, *108*, 357.

(21) dePaola, R. A.; Hrbek, J.; Hoffman, F. M. *J. Chem. Phys.* **1985**, *82*, 2484.

(22) Gerlach, R. L.; Rhodin, T. N. *Surf. Sci.* **1969**, *17*, 32.

(23) Anderson, S.; Jostell, U. *Solid State Commun.* **1973**, *13*, 829.

(24) Redhead, P. A. *Vacuum* **1962**, *12*, 203.

(25) "CRC Handbook of Chemistry and Physics"; Chemical Rubber Co.: Cleveland, 1968-69; 49th ed.

(26) Zachariasen, W. H. *J. Inorg. Nucl. Chem.* **1973**, *35*, 3487.

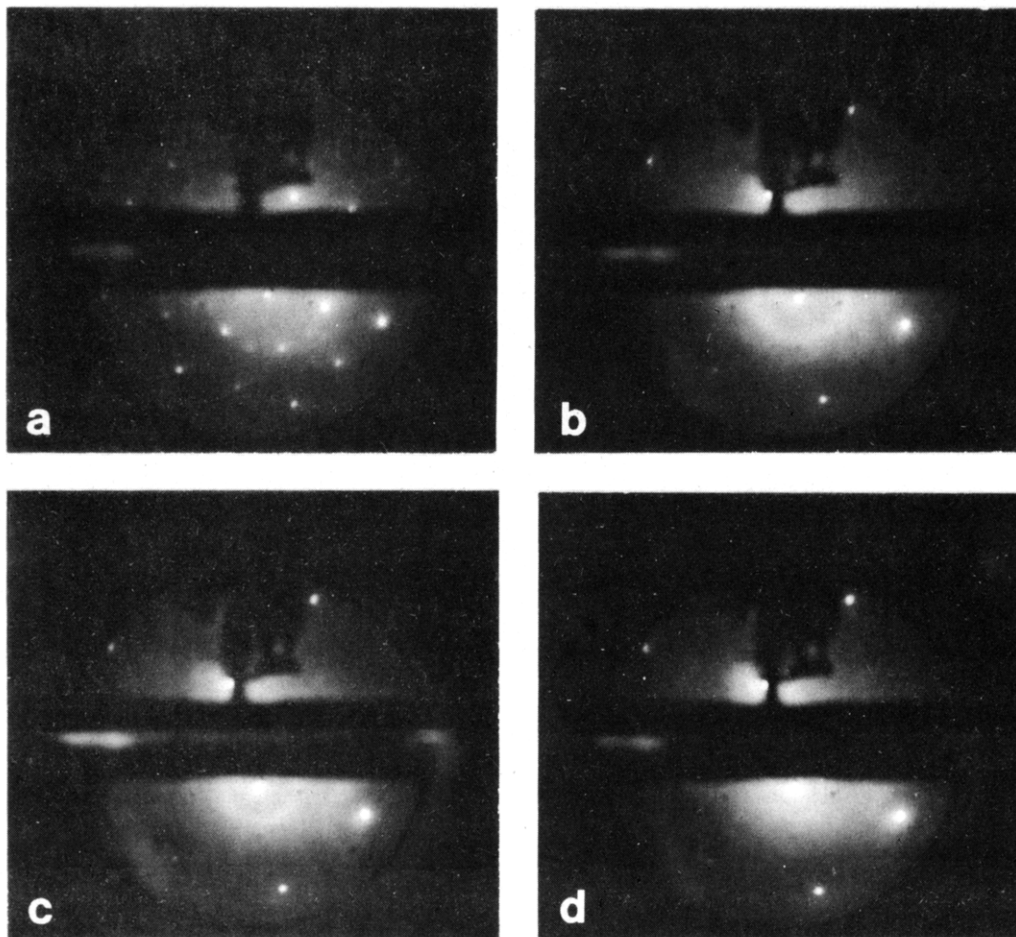


Figure 3. LEED patterns for Cs overlayers on clean Ag(111). (a) p(2x2) pattern obtained by room temperature saturation or by flashing higher coverages deposited below room temperature to 320 K to remove multilayers ($\theta_{Cs} = 0.25$). (b-d) Ring patterns obtained after flashing (a) to increasing temperatures to remove Cs: (b) 539 K, $\theta_{Cs} = 0.14$, $\theta_{Cs}^{LEED} = 0.18$, (c) 611 K, $\theta_{Cs} = 0.10$, $\theta_{Cs}^{LEED} = 0.11$, and (d) 683 K, $\theta_{Cs} = 0.08$, $\theta_{Cs}^{LEED} = 0.08$. Conditions: incident beam a few degrees off normal; beam energies of 84, 95, 95, and 95 eV, respectively; patterns photographed at ~ 200 K.

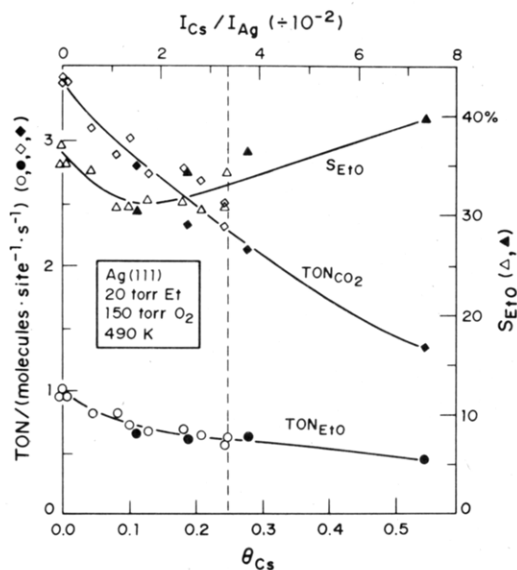


Figure 4. Steady-state (low conversion) rates of ethylene oxide (EtO) and CO₂ production from a mixture of 20 torr of ethylene and 150 torr of O₂ for various Cs predeposited coverages on Ag(111) at 490 K. Also shown is the selectivity (S_{EtO}) variation. Difference between filled and open symbols described in section III.3.

for the clean surface, for the surface containing near saturation Cs exposures at 300 K, and for these same Cs-dosed surfaces after steady-state reaction at $P_{Et} = 20$ torr, $P_{O_2} = 150$ torr, and 490 K. After reaction, a strong O(KVV) signal is observed. This has a line shape significantly different than that for atomically ad-

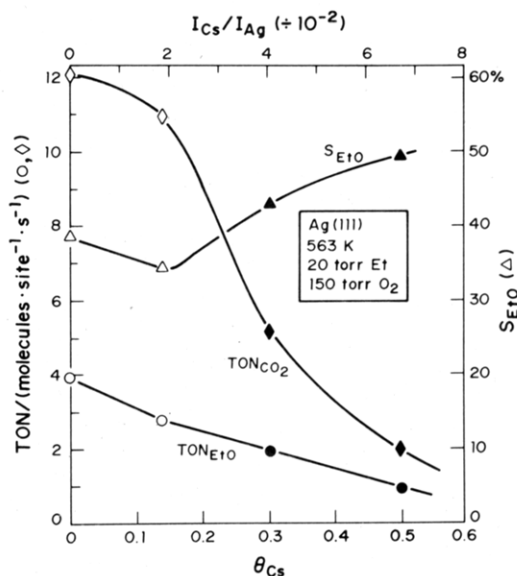


Figure 5. Same as Figure 4, at 563 K.

sorbed oxygen (O_a) on Ag(111).^{27,28} The clean surface shows a very tiny amount of O_a ($\theta_0 < 0.01$) after reaction at these conditions.¹⁴ A p(4x4)-O overlayer ($\theta_0 \approx 0.41$) on Ag(111) gives an O/Ag AES ratio of 0.020 on this same spectrometer.²⁷ Using this calibration point, our present data indicate oxygen coverages after reaction of $\theta_0 = 0.70$ and 0.78 for initial coverages $\theta_{Cs} =$

(27) Campbell, C. T. *Surf. Sci.* **1985**, *157*, 43.

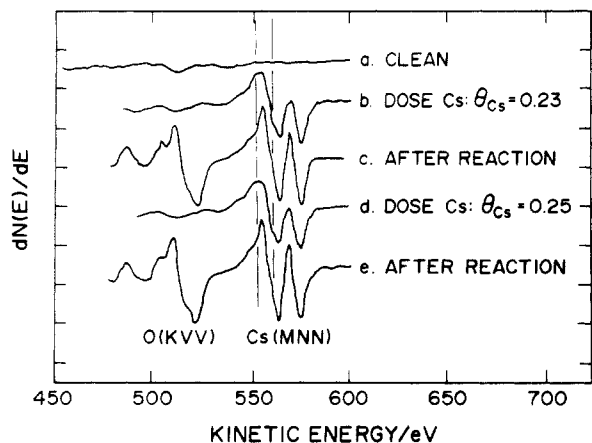


Figure 6. AES spectra of (a) clean Ag(111), (b, d) after dosing Cs to the clean surface, and (c, e) the same surfaces after steady-state epoxidation reaction at the conditions of Figure 4. Note the Cs line shapes changes near the vertical lines induced by reaction.

0.23 and 0.25, respectively. These values are considerably higher than the saturation coverage for O_2 on clean Ag(111) ($\theta_0 \approx 0.41$).²⁷

The O/Cs AES ratio after reaction was 0.78 ± 0.1 , relatively independent of Cs coverage. This indicates that a Cs/O "compound" forms on the Ag surface during reaction which has a stoichiometry of CsO_x where $x = 3.1 \pm 0.4$. (Here we have used a Cs/O AES atomic sensitivity ratio of 4.0, obtained by comparing the O/Ag and Cs/Ag AES ratios for the $p(4 \times 4)$ -O and $p(2 \times 2)$ -Cs structures.) Note in Figure 6 that the Cs(MNN) AES line shape changes significantly by reaction, so that its peak-to-peak height increases by a factor of ~ 1.5 . (This has been accounted for in the above calculation of stoichiometry.) The line shape change indicates a change in the chemical nature of the Cs. After reaction, the line shape is similar to that reported for ionically bonded Cs (CsI),²⁹ showing a maximum at ~ 570 eV considerably above the base line. Note the shoulders at ~ 552 and 560 eV for clean Cs/Ag(111), identified with vertical markers in Figure 6.

The Cs TDS looks very different after reaction, as shown in curves a-d of Figure 7. With increasing θ_{Cs} , a doublet (α, β) first appears at ~ 600 K. The doublet reaches its maximum intensity at rather low Cs coverages ($\theta_{Cs} \approx 0.1$). Then a peak (γ) near 720 K grows. All peaks shift to higher temperature with increasing Cs coverage. Desorbing nearly simultaneously with the (α, β) Cs doublet was an O_2 doublet at m/e 32, as shown in curve f of Figure 7. Oxygen removal was nearly complete by 650 K as indicated here and also by repeating this experiment but halting the TDS at 650 K for AES observation. The removal of Cs was not complete by 650 K, however, as seen by the γ -Cs TDS peak and by AES. We did not monitor for gaseous Cs oxides.

The simultaneous desorption of Cs and O_2 at ~ 600 K is evidence for the decomposition of a Cs/O surface compound. Based on the above AES results, we will take its stoichiometry to be CsO_3 . In this compound, oxygen is stabilized with respect to O_a on clean Ag(111), which desorbs as O_2 in a single peak at 580 K.²⁷ Curve e of Figure 7 shows that if the α -Cs TDS state is removed by flashing just to 600 K, it reappears in the subsequent TDS. This indicates facile transfer between these two Cs/O states.

This CsO_3 surface compound gives a sharp $(2\sqrt{3} \times 2\sqrt{3})R30^\circ$ LEED pattern, as seen in Figure 8a-c. Note that the spots expected for this pattern nearest the (0,0) beam were not observable; and the spots such as $(1/2, 1/2)$ are at best only barely visible. By comparing parts a and b of Figure 8, this LEED pattern is stable over a large range of initial Cs coverages. The overlayer spot intensity grows with θ_{Cs} , indicating that the CsO_3

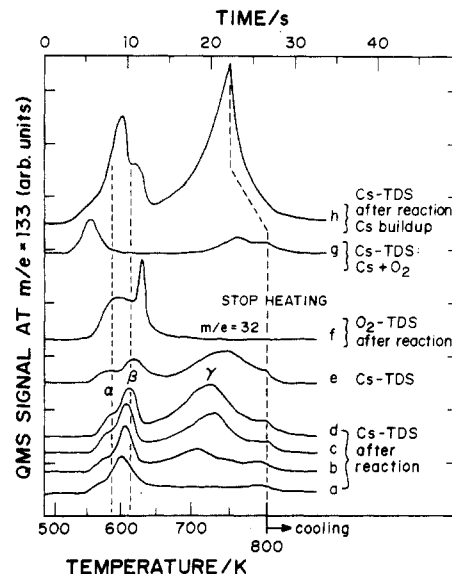


Figure 7. (a-d) Cs TDS after steady-state epoxidation reaction at 490 K, $P_{Et} = 20$ torr, and $P_{O_2} = 150$ torr for various Cs/Ag(111) overlayers. Predosed Cs coverages were $\theta_{Cs} = 0.05, 0.10, 0.14,$ and 0.19 , respectively. (f) Same as above, $\theta_{Cs} = 0.25$, only here we follow the m/e 32 O_2 signal instead of Cs desorption. (e) Same as (a-d), $\theta_{Cs} = 0.22$, only here the surface after reaction was first flashed to 600 K to remove just the α -Cs TDS peak. The reappearance of this state indicates rapid $\alpha \rightleftharpoons \beta$ state conversion. (h) Cs TDS following reaction for a large Cs coverage: AES ratio $I_{Cs}/I_{Ag} = 0.074$, corresponding to $\theta_{Cs} \approx 0.56$. Method of obtaining this high coverage described in text. (g) Cs TDS from a $(2\sqrt{3} \times 2\sqrt{3})R30^\circ$ Cs/O overlayer obtained, as described in text, by dosing O_2 in the UHV chamber to Cs/Ag(111).

surface compound coalesces into two-dimensional islands of this $(2\sqrt{3} \times 2\sqrt{3})R30^\circ$ structure. This would leave regions of the surface relatively free of Cs at low initial Cs exposures.

The $(2\sqrt{3} \times 2\sqrt{3})R30^\circ$ pattern reverted to a $p(1 \times 1)$ pattern upon briefly heating in UHV to ~ 630 K to desorb the (α, β) Cs and O_2 TDS doublet. This pattern is therefore clearly associated with this (α, β) doublet, rather than the γ -Cs state at ~ 750 K. We should note that, after reaction, we were not able to cool below room temperature for LEED observation. The $p(1 \times 1)$ pattern mentioned here may have shown structure if cooled below room temperatures, since clean Cs/Ag(111) required low temperatures for LEED observations (see above). There is evidence that the Cs desorbing above ~ 630 K after reaction was partially dissolved below the surface of the Ag and therefore inaccessible to AES. When an initial coverage $\theta_{Cs} = 0.22$ ($I_{Cs}/I_{Ag} = 0.029$) was run at steady-state reaction conditions as in Figure 4, and then flashed to ~ 630 K in UHV, the remaining Cs/Ag AES ratio was 0.013. This is only 45% of its initial value, whereas the TDS spectra such as Figure 7d indicate that $>70\%$ of the Cs remains undesorbed at this temperature. The Cs AES line shape reverted to that for a pure Cs overlayer after flashing to 630 K to remove the oxygen. When such a surface is returned to the microreactor and a steady-state reaction condition is established (Figure 4 conditions), Cs moves out of the desorption states above 630 K and back into the (α, β)-TDS doublet. The $(2\sqrt{3} \times 2\sqrt{3})R30^\circ$ LEED pattern is also regenerated. The reaction rates are not much different for this surface than for a surface dosed as usual with Cs to this same AES level (compared after reaction). The selectivity was slightly ($\sim 5\%$ absolute units) higher.

III.3. Reaction Studies for $\theta_{Cs} > 0.25$. Since the rates and selectivity were not greatly effected by a saturation dose of Cs at 300 K ($\theta_{Cs} = 0.25$), we considered the possibility that the surface was not completely saturated in the CsO_3 compound after establishing reaction conditions. For this reason we attempted to push our kinetic measurements to higher Cs levels by dosing Cs to a surface which already contained the " $2\sqrt{3}$ " Cs/O surface compound generated by a previous reaction sequence. The addition of Cs to this " $2\sqrt{3}$ " structure generally destroyed the $(2\sqrt{3} \times 2\sqrt{3})R30^\circ$ pattern, leaving only $p(1 \times 1)$ spots and higher

(28) Campbell, C. T.; Paffett, M. T. *Surf. Sci.* **1984**, *143*, 517.

(29) Davis, L. E.; MacDonald, N. C.; Palmberg, P. W.; Riach, G. E.; Weber, R. E. "Handbook of Auger Electron Spectroscopy"; Physical Electronics Division, Perkin Elmer: Eden Prairie, MN, 1976.

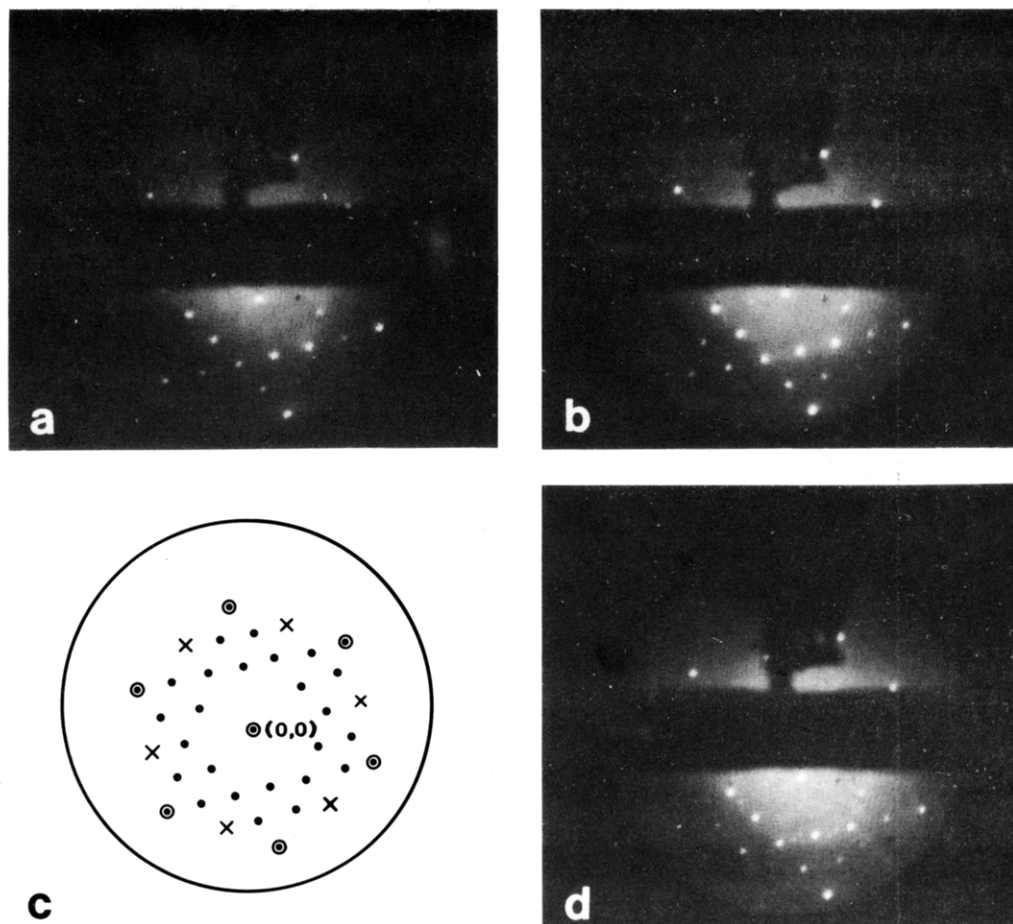


Figure 8. $(2\sqrt{3} \times 2\sqrt{3})R30^\circ$ LEED patterns for Cs/O structures after high-pressure epoxidation reactions over Cs/Ag(111). (Reaction conditions same as Figure 7a–d.) (a) $\theta_{Cs} = 0.11$, (b) $\theta_{Cs} = 0.27$, (c) schematic representation of $(2\sqrt{3} \times 2\sqrt{3})R30^\circ$ pattern showing Ag(111) substrate spots (\odot), overlayer spots (\bullet), and spots which are extremely weak (\times). (Spots expected nearest the (0,0) reflection were generally not observed.) (d) $\theta_{Cs} = 0.56$, showing additional complex spots obtained at very high Cs coverages after reaction. Conditions: incident beam a few degrees off normal; beam energy near 70 eV; photographed at ~ 310 K.

background. The kinetic results are shown in Figures 4 and 5 as the filled symbols, which are plotted at the ratio I_{Cs}/I_{Ag} measured immediately after the final Cs dose (before final reaction). As shown, we made several measurements in this way for $\theta_{Cs} < 0.25$ for comparison with the single-dose results of section III.2. The good agreement indicates that either method of preparing a Cs overlayer results in the same structure and reactivity under steady-state reaction conditions. The results for $\theta_{Cs} > 0.25$ can therefore be trusted as representative. Note that the selectivity to ethylene epoxide can be significantly enhanced at large Cs coverages.

After reaction, such a surface showed a Cs TDS which had significantly increased population in both the α - and γ -state desorption regions, as seen in Figure 7h for $I_{Cs}/I_{Ag} = 0.074$. The area under the Cs TDS peaks is much larger than is indicated by this AES ratio, suggesting that some of the Cs here is below the probe depth of the Auger electrons. As noted above, this may be due to the fact that the Cs desorbing near 750 K is actually coming from Cs dissolved in the Ag crystal. Such a model is consistent with the strong shift to higher temperatures of the γ -TDS peak with increasing coverage. This is characteristic of a desorption rate which is limited by the diffusion concentration profile.

After epoxidation reactions using these high Cs levels at 563 K such as in Figure 5, both the β - and γ -Cs TDS peaks were shifted considerably (~ 40 K) to higher temperature compared to reaction at 490 K. The details of these differences have not been pursued. The higher reaction temperature may drive Cs deeper into the bulk, giving a broadened concentration profile and an increase in the γ -peak temperature.

The high-coverage Cs/O surface giving rise to the TDS in Figure 7h gave the LEED pattern of Figure 8d after reaction at

490 K. This pattern has a strong $(2\sqrt{3} \times 2\sqrt{3})R30^\circ$ component characteristic of lower θ_{Cs} , as well as additional faint triplets as shown. We will not attempt to interpret this structure. Coverages below $\theta_{Cs} = 0.4$ in Figures 4 and 5 gave only a good $(2\sqrt{3} \times 2\sqrt{3})R30^\circ$ LEED pattern after reaction. We should point out that for initial Cs coverages above 0.25, the Cs level decreased during reaction, so that, for example, the point at $\theta_{Cs} = 0.56$ in Figure 4 had a Cs AES signal corresponding to $\theta_{Cs} = 0.36$ after reaction. (We considered the AES line shape change to obtain this value.)

III.4. Oxygen Adsorption on Cs/Ag(111). The interaction of O_2 with a Cs-dosed Ag(111) surface has already been studied to some extent,¹⁶ although no LEED structures were reported. Due to the obvious significance of the $(2\sqrt{3} \times 2\sqrt{3})R30^\circ$ -O/Cs structure to the promotion of Ag catalysts by Cs, we were interested to know whether this structure could be generated by simple O_2 dosing in a UHV chamber. If so, it would be much more attractive for future, more detailed surface structural analyses. We performed a limited number of experiments to test this question. We found that indeed the $(2\sqrt{3} \times 2\sqrt{3})R30^\circ$ pattern could be generated in UHV by dosing O_2 to a Cs overlayer.

First, Cs was dosed to clean Ag(111) up to a coverage $\theta_{Cs} = 0.11$ at room temperature. Then we dosed 250-langmuir (1 langmuir = 10^{-6} torr s) O_2 at room temperature. This gave an O/Cs AES ratio of 1.16 and an increased Cs/Ag ratio (0.0173). This was then briefly flashed to 490 K. The O/Cs AES decreased to 0.65. This surface showed a faint $(2\sqrt{3} \times 2\sqrt{3})R30^\circ$ LEED pattern. A further 250-langmuir O_2 dose at room temperature followed by a flash to 490 K did not significantly change the O or Cs AES signals (Cs/O = 0.67, Cs/Ag = 0.016), but gave a good, sharp $(2\sqrt{3} \times 2\sqrt{3})R30^\circ$ LEED pattern. This surface gave the Cs TDS shown in Figure 7g. While this spectrum is not the

same as that seen after reaction (Figure 7a-d), there are strong similarities. The (α,β) doublet has been replaced by a singlet at somewhat lower temperature (~ 555 K). A higher initial Cs coverage ($\theta_{\text{Cs}} = 0.23$) shifted this singlet up to ~ 600 K and gave much greater intensity in the Cs desorption peak near 770 K. The important point here is that the $(2\sqrt{3} \times 2\sqrt{3})\text{R}30^\circ\text{-Cs/O}$ structure can be generated by Cs + O₂ dosing in UHV. We did not attempt to optimize the recipe for its preparation. A similar Cs/O complex has recently been observed on Ag(110).³⁷

IV. Discussion

IV.1. Cesium Adsorption. The thermal desorption spectra for Cs shown in Figure 2 are similar to those reported by Grant and Lambert¹⁶ for Ag(111) up to about 600 K. However, they did not report any significant desorption above about 600 K, whereas we see structureless desorption up to above 800 K. The reason for this discrepancy is not clear. As mentioned above, Cs desorption continues up to about 1100 K on Ni surfaces.¹⁸ In the case of Ag(111), it seems clear that this Cs resides on the surface, since the characteristic "ring" LEED patterns were seen for surfaces heated to 611 K to remove the lower temperature desorption states (Figure 3, c and d).

Comparing the evolution of thermal desorption line shapes (for $T < 650$ K) with coverage, our present Cs coverage calibration agrees well with that used by Grant and Lambert based upon integrated "positive surface ionization" currents.¹⁶ However, these authors suggested that the first layer of Cs completes at $\theta_{\text{Cs}} = 0.13$ and that two layers of Cs exist at $\theta_{\text{Cs}} = 0.25$. This was based upon a break seen in the curve for the 47-eV Cs AES signal vs. coverage. We saw no distinct break in the 563-eV Cs signal (Figure 1). Furthermore, the small amount of attenuation of the 351-eV Ag AES signal (Figure 1) at $\theta_{\text{Cs}} = 0.25$ (78% of bulk signal) is entirely inconsistent with two layers of Cs. Since Cs has a metallic diameter of ~ 5.3 Å, two layers would have a thickness of ~ 8.2 Å (assuming close packing). To account for only 22% attenuation of the Ag AES signal, this thickness would then require a mean-free path (λ) of >33 Å for the 351-eV Auger electrons. Reported values for λ fall within the range 5–20 Å,³⁰ much more consistent with a single Cs layer thickness. It is possible that the change in slope seen by Grant and Lambert¹⁶ for the 47-eV Cs AES signal is due to electronic effects on the line shape, such as shown in Figure 6, where ionic Cs gives a signal 50% stronger than metallic Cs. Note that alkali adsorption shifts from ionic to metallic within the first monolayer,^{18–23} giving rise to a minimum in work function vs. coverage. Also, due to the large work function change expected within the first layer,^{18–23} large changes in the secondary electron distribution near the onset (<50 eV) are expected. This could also disturb the 47-eV Cs peak-to-peak height.

We also note that the $p(2 \times 2)\text{-Cs}$ LEED pattern seen at $\theta_{\text{Cs}} = 0.25$ is consistent with a close-packed single layer of Cs adatoms. The "ring" pattern diameters at lower coverages (Figure 3b-d) are also consistent with our coverage calibration. Previous studies of Cs adsorption on other transition metals also conclude that adsorption at 300 K completes in a single layer of about this same density.^{31,32}

IV.2. Epoxidation Kinetics on Cs/Ag(111). Under the conditions of our measurements, Cs always tends to decrease the activity for both EtO and CO₂ production with respect to clean Ag(111) (Figures 4 and 5). The similarity in the data at 490 and 563 K indicates that Cs induces no major change in the activation energy of the rate-determining step for either EtO or CO₂ production in this range of conditions. This is to be contrasted with work by Grant and Lambert,¹⁶ where Cs caused a slight increase in activity up to $\theta_{\text{Cs}} \approx 0.25$, above which the activity decreased. These authors also reported just the opposite trends in selectivity with θ_{Cs} to that which we observe. The difference may be due

to the fact that their ethylene and O₂ pressures (5 torr) were much lower than we have used.

The reason that Cs is added to industrial catalysts is to increase selectivity, perhaps at the expense of some loss in activity.¹ This is consistent with our results for Ag(111) when θ_{Cs} exceeds 0.15. Since our results are for a bulk Ag sample, we see that Cs can enhance selectivity even in the absence of a support material such as Al₂O₃. Thus direct Cs-Ag interactions will be important in understanding completely the role of Cs promoters, although effects on the support may also be important. Furthermore, since our results represent very low conversion where further oxidation of the epoxide product is negligible,^{6,7} any complete explanation of the selectivity enhancement must concern Cs effects on the forward rates of EtO and CO₂ production. Here, Cs decreases the rate of CO₂ production more rapidly than that of EtO production, leading to an enhanced selectivity.

IV.3. Surface Structure after Reaction. Mutual Cs-O ionic attractions stabilize adsorbed Cs to much higher coverages than would otherwise be stable at the elevated reaction temperatures. In fact, a surface oxide of stoichiometry $\sim \text{CsO}_3$ is formed, and coalesces into islands of a $(2\sqrt{3} \times 2\sqrt{3})\text{R}30^\circ$ structure. This structure decomposes at ~ 600 K to yield Cs and O₂ gas. Oxygen adatoms (O_a) associatively recombine to form O₂ gas on clean Ag(111) at about 580 K.²⁷ The similarity of these temperatures suggests that this complex might most appropriately be viewed as a mutual stabilization of adsorbed Cs and atomic oxygen where the dominate bonding for oxygen is still to the Ag substrate. Similar models are used to explain K/CO interactions and stoichiometry on metal surfaces.²¹ The true nature of this interaction will await detailed study of the structural and electronic properties of this complex. In the absence of this interaction, only very low Cs coverages would be stable at the reaction temperatures. Without knowledge of this extra stabilization, one might falsely assume that essentially all the Cs promoter must locate on the catalyst support (Al₂O₃).

On Cs-dosed Ag(111), oxygen coverages (in this Cs-O surface complex) can approach $\theta_0 = 1$ under reaction conditions. In contrast, clean Ag(111) shows an O_a coverage of only a few percent at these same reaction conditions.¹⁴ Since O_a desorption as O₂ is very slow compared to its removal rate via reaction at 490 K even on clean Ag(111),^{11,14,28} this large increase in O_a coverage is not directly due to the increased thermal stability of O_a in the presence of Cs. Instead, this is due to the increase in its formation rate. The initial dissociative sticking probability for O₂ on Ag(111) increases from $\sim 10^{-6}$ (ref 27) to near unity (ref 16 and 33 and present work) upon Cs addition.

In spite of this huge increase in the rate of O_a formation, the overall catalytic reaction rates decrease upon Cs addition. This is consistent with our earlier results,^{10–15,34} which indicated a reaction mechanism wherein adsorbed ethylene and molecularly adsorbed O₂ (not O_a) combine in the rate-determining step. We note that under the conditions of Figures 4 and 5, the reaction rate is positive order in P_{O_2} ^{10,13} and therefore to some extent limited by the supply of oxygen into its reacting form.

In terms of the influence of Cs upon the reaction kinetics, it appears that this Cs/O complex acts much like Cl adatoms:^{12,13,34} the rates decrease and the selectivity increases at high coverage. We have shown that chlorine increases the selectivity by changing a branching ratio for decomposition of a C₂H₄-O₂ complex after the rate-determining step.¹³ The effect on the branching ratio required an explanation involving ensemble size requirements rather than electronic interactions. Ensemble effects should also arise due to the presence of this Cs/O complex, and a similar explanation could be appropriate here.

Our conclusion of a stoichiometry of CsO₃ after reaction is based on the fixed Cs/O AES ratio, where the relative Cs and O sensitivities were calibrated based upon LEED patterns for overlayers of the separate elements. We feel that this calibration is quite good. Ayyoob and Hedge have found by calibrated XPS

(30) Seah, M. P.; Dench, W. A. *Surf. Interface Anal.* **1979**, *1*, 2.

(31) Lindgren, S. A.; Wallden, L. *Phys. Rev. B* **1980**, *22*, 5967. *Surf. Sci.* **1979**, *80*, 620.

(32) Papageorgopoulos, C. A. *Phys. Rev. B* **1982**, *25*, 3740.

(33) Ayyoob, M.; Hedge, M. S. *Surf. Sci.* **1983**, *133*, 516.

(34) Campbell, C. T. *J. Catal.*, in press.

intensities a saturation oxygen concentration of about three times θ_{Cs} for O_2 adsorption on Cs-dosed Ag,³³ consistent with our result. However, if one uses the relative AES sensitivities tabulated in the Phi Handbook for Cs/O,²⁹ one obtains a stoichiometry of $\sim\text{Cs}_3\text{O}$, much different than these results. This indicates that the tabulated AES sensitivities for Cs or O^{29} may be in error by as much as a factor of 8. Line shape differences such as shown in Figure 6 might be a large contributor to this problem. Crude calculations for our pure Cs or oxygen reference overlayers based upon mean-free-paths indicate that the largest error lies in the Cs sensitivity (factor of ~ 4).

The large line shape change seen for the ~ 560 -eV Cs AES peak upon oxidation is somewhat interesting. This transition is typically labeled MNN,²⁹ that is, one involving three core levels of the Cs atoms. One might expect only a uniform shift of these core levels, resulting in a shift of the AES peak³⁵ without significant change in the detailed line shape. Line shape changes are usually expected for peaks involving valence levels.³⁵ Interestingly, this AES peak energy could also contain significant $\text{M}_{4,5}\text{N}_{2,3}$ V contributions, as the $\text{M}_{4,5}$ and $\text{N}_{2,3}$ levels are separated by about 554–588 eV. The additional contribution of this MNV transition may be complicating the tabulated AES sensitivity.

Due to the complexity within the $(2\sqrt{3} \times 2\sqrt{3})\text{R}30^\circ$ unit cell, we will not present a structural model for that CsO_3 LEED pattern. There may be similarities to the postulated model for a $\text{K}(\text{CN})_4$ $(2\sqrt{3} \times 2\sqrt{3})\text{R}30^\circ$ pattern on Pt(111).³⁶ Any model must include about four CsO_3 units per unit cell. The high

epoxidation activity for a surface essentially saturated in this structure suggests that the model should perhaps involve Ag atoms available for bonding on the surface. A detailed structural analysis of this pattern would be welcomed.

V. Conclusions

In this preliminary investigation of the role of Cs promoters in Ag catalysts for ethylene epoxidation, we have learned that this is a very complicated system. It will require considerable study before characterization is complete. There are a number of important conclusions, however, which can now be drawn.

Cesium is adsorbed ionically at low coverages on Ag(111), with strong lateral repulsions. The thermal stability of Cs on Ag is greatly enhanced under reaction conditions due to the formation of a Cs/O surface structure showing a $(2\sqrt{3} \times 2\sqrt{3})\text{R}30^\circ$ LEED pattern. The stoichiometry of this structure is near CsO_3 . Its formation is very rapid and can also be accomplished with small doses of O_2 gas to Cs/Ag(111) in UHV conditions. It decomposes near 600 K in UHV, yielding nearly simultaneous desorption of O_2 and Cs gas. Above this temperature some Cs remains, partially dissolved below the Ag surface. This Cs desorbs above 700 K. The addition of Cs causes a decrease in the catalytic rates of both ethylene oxide and CO_2 production compared to clean Ag(111). The selectivity decreases at low θ_{Cs} , then increases to values higher than the clean surface. These results have significant implications for industrial processes where Cs promoters are added to Ag catalysts.

Acknowledgment. The author thanks Gabor Somorjai for pointing out the importance of cesium promoters in this reaction.

Registry No. Ag, 7440-22-4; Cs, 7440-46-2; O_2 , 7782-44-7; ethylene, 74-85-1.

(35) Madden, H. H. *J. Vac. Sci. Technol.* **1981**, *18*, 677.

(36) Stickney, J. L.; Rosasco, S. D.; Salaita, G. N.; Hubbard, A. T. *Langmuir* **1985**, *1*, 66.

(37) Prince, K. C.; Kordesch, M. E. *Appl. Surf. Sci.* **1985**, *22/23*, 469.

Detailed Aspects of Raman Scattering. Overtone and Combination Intensities and Prescriptions for Determining Excited-State Structure

David E. Morris and William H. Woodruff*

Los Alamos National Laboratory, University of California, Los Alamos, New Mexico 87545

(Received: June 27, 1985)

The time-dependent theory of resonance Raman scattering developed by Heller and co-workers is extended to a more general case which considers simultaneous occurrence of excited-state normal-coordinate displacements, force-constant changes, and Duschinsky rotation upon resonant electronic excitation. General expressions are developed for ground-state scattering intensities (fundamentals, overtones, and combinations) in terms of excited-state structural and force-field parameters. It is shown that all factors contributing to the intensities must be considered if accurate excited-state parameters are to be obtained from experimental data. In particular, additional terms which were not explicitly developed in the earlier treatments can dramatically influence the calculated overtone and combination intensities. The results are applied to the redetermination of the displacement of the Mo–Mo coordinate in the $\delta \rightarrow \delta^*$ excited state of quadruply bonded $\text{Mo}_2(\text{O}_2\text{CR})_4$, and compared to an earlier determination which employed a simplified form of the theory.

Introduction

Recent developments by Heller and co-workers¹ in the time-dependent, semiclassical theory of Raman scattering are of enormous potential value in determining structural and vibrational parameters of species in excited electronic states. Experimental measurements of *ground-state* Raman intensities of fundamentals, overtones, and combinations under resonance or near-resonance conditions can be used to deduce normal-coordinate displacements, force-constant changes, and normal-mode mixing (Duschinsky rotation) in the excited state. This approach to the determination

of excited-state structures and force fields is particularly attractive because it does not require direct observation of excited-state vibrational frequencies by time-resolved vibrational spectroscopies (TRVS) or resolved vibronic spectroscopies. Thus, Heller theory analysis of ground-state Raman data is not subject to limitations imposed by short excited-state lifetimes or other conditions which may hamper TRVS measurements, nor is it limited by the often experimentally stringent conditions under which resolved vibronic spectra are obtained. Further, in cases where TRVS and/or vibronic data are available, Heller theory analysis affords an additional test of the accuracy of calculated excited-state parameters.

Existing explicit mathematical treatments are limited to the "simple aspects of Raman scattering"^{1a} wherein special cases in the relationship between ground- and excited-state structures and

(1) (a) Heller, E. J.; Sundberg, R. L.; Tanner, D. *J. Phys. Chem.* **1982**, *86*, 1822–1833. (b) Tannor, D. J.; Heller, E. J. *J. Chem. Phys.* **1982**, *77*, 202–218. (c) Lee, S. Y.; Heller, E. J. *J. Chem. Phys.* **1977**, *71*, 4777–4788. (d) Heller, E. J. *Acc. Chem. Res.* **1981**, *14*, 368–375.